Journal of Breast Cancer

J Breast Cancer 2016 June; 19(2): 191-198 http://dx.doi.org/10.4048/jbc.2016.19.2.191

ORIGINAL ARTICLE

Breast Magnetic Resonance Imaging for Assessment of Internal Mammary Lymph Node Status in Breast Cancer

Hyung Won Lee, Sung Hun Kim

Division of Radiology, Seoul St. Mary's Hospital, The Catholic University of Korea College of Medicine, Seoul, Korea

Purpose: The purpose of this study was to assess magnetic resonance imaging (MRI) features of malignant internal mammary lymph nodes (IMLNs) and benign IMLNs in breast cancer patients. **Methods:** From 2009 to 2014, the records of 85 patients with IMLNs were archived using MRI report data; 26 patients with small size (long axis diameter <5 mm) nodes were subsequently excluded. The current study evaluated internal mammary lymph nodes in 59 patients who underwent breast MRI for breast cancer staging and for posttherapy follow-up. All MRI findings were retrospectively evaluated. Malignancy was determined based on pathologic examination and positron emission tomography computed tomography findings. Independent t-tests, Mann-Whitney U tests, chi-square tests, and receiver operating characteristics (ROC) curve analysis were used. **Results:** Among MRI features, there were statistically significant differences between benign and malignant IMLN groups, in short axis length (3.6±1.3 vs. 8.2±2.9 mm, respectively), long axis length (8.1±2.4 vs. 14.5±4.8 mm, respectively), short/long axis ratio (0.45±0.10 vs. 0.59±0.17, respectively), absent fatty hilum (mean, 0% vs. 95%, respectively), and restricted diffusion (15.8% vs. 85.0%, respectively) ($p<0.050$). Multiplicity and location of intercostal spaces was not different between the two groups. Short axis length was the most discriminative variable for predicting metastatic nodes (area under the ROC curve, 0.951; threshold, 4 mm; sensitivity, 92.5%; specificity, 84.2%). **Conclusion:** Conventional MRI and diffusion-weighted MRI are helpful to detect metastasis of internal mammary lymph nodes in breast cancer.

Key Words: *Breast neoplasms, Lymph nodes, Magnetic resonance imaging, Neoplasm metastasis*

INTRODUCTION

Internal mammary lymph nodes (IMLNs) are a secondary lymphatic drainage area in breast cancer. IMLN metastases occur in 16.7% to 40% of breast cancer patients, who show shorter survival rates than breast cancer patients overall [1]. While the prognostic significance of IMLN metastasis is well known, the management of IMNLs in breast cancer remains controversial in the field of oncology. Surgical procedures for sampling internal mammary lymph nodes carry the risk of bleeding, are time consuming, and require advanced surgical experience. Several trials have failed to prove the advantage of surgical dissection of IMLNs for disease-free and overall survival [2,3]. However, others posit that knowing the pathological status of IMLNs could help with tumor/node/metastasis (TNM) staging and in the development of an appropriate treatment strategy to control local lesions and improve the patients' quality of life. A positive IMLN biopsy would be an indication for adjuvant internal mammary radiotherapy as well as adjuvant systemic treatment [4-6].

Recent evidence indicates that ultrasound imaging (US)-guided core-needle biopsy or fine-needle aspiration performed on suspicious IMLN metastases could yield a high success rate without serious complications [7]. Although mammography, US, and magnetic resonance imaging (MRI) are used for breast imaging, the optimal imaging modalities or diagnostic criteria for detection of IMLN metastasis have not been established [8]. Historically, MRI has been considered the most sensitive imaging modality for the detection and assessment of breast cancer, but to our knowledge, there is only one report in the literature describing a statistical analysis of the use of MRI to detect malignant IMLNs. Kinoshita et al. [9] reported that, using size-based criterion (defining ≤5 mm as positive), MRI had 90.7% accuracy, 93.3% sensitivity, and 89.3% specificity, with no significant differences in shape- or margin-based criteria. As the role of MRI in evaluating pa-

Correspondence to: **Sung Hun Kim**
Division of Radiology, Seoul St. Mary's Hospital, The Catholic University of Korea College of Medicine, 222 Banpo-daero, Seocho-gu, Seoul 06591, Korea
Tel: +82-2-2258-6250, Fax: +82-2-2258-1457
E-mail: rad-ksh@catholic.ac.kr

Received: December 10, 2015 **Accepted:** February 28, 2016

http://ejbc.kr | pISSN 1738-6756
eISSN 2092-9900

tients with breast cancer expands, a better understanding of MRI findings of IMLNs is needed to enable correct preoperative diagnosis and appropriate management.

The purpose of this study was to describe MRI features of malignant and benign IMLNs and to determine the most effective parameter for detecting metastatic IMLNs in breast cancer patients.

METHODS

This study was approved by Seoul St. Mary's Hospital Institutional Review Board (KC15RISI0092) and the need for informed consent was waved.

Patients

Based on a review of breast MRI records from May 2009 to December 2014, 85 patients with IMLNs were identified. Twenty-six patients were excluded because the lesions were too small (long axis diameter < 5 mm) to characterize. The remaining 59 patients were classified into the malignant IMLN group (n = 40) or benign IMLN group (n = 19). This classification procedure was achieved in several ways. In 10 cases, benignity (n = 1) and malignancy (n = 9) were determined using pathologic examination. If pathologic examination was not performed, benign IMLNs were defined as showing 1 year of stability on MRI or no fluorodeoxyglucose (FDG) uptake on positron emission tomography computed tomography (PET/CT) (n = 18). In contrast, malignant IMLNs were defined as showing FDG uptake greater than that of the adjacent background activity (determined in regions such as the pectoralis muscle, the intercostal space along the lateral sternal border or the mediastinal blood pool), increased FDG uptake on follow up PET/CT, an increased in size during the follow-up period, or a decrease in size after chemotherapy or radiation treatment (n = 31) [7,10].

Patient pathologic and medical reports were reviewed for tumor size, axillary lymph node (LN) status, and distant metastasis.

MRI technique

MRI was performed in the prone position using a dedicated bilateral breast surface coil. Imaging with a 3T MRI system (Verio; Siemens Healthcare, Erlangen, Germany) was obtained using the following sequences: (1) an axial, turbo spin-echo T2-weighted imaging sequence with repetition time/echo time (TR/TE) of 4,530/93, flip angle of 80°, 34 slices, field of view (FOV) of 320 mm, matrix size of 576 × 403, 1 number of excitations (NEX), slice thickness of 4-mm and acquisition time of 2 minutes 28 seconds; (2) axial diffusion weighted imaging (DWI) with two sequences (i.e., single-shot echo planar image [ss-EPI] or readout segmented EPI [rs-EPI]) (b values, 0 and 750 s/mm^2; TR/TE, 9,800/87 ms and 5,600/55 ms, respectively; FOV, 340 × 117 mm and 360 × 180 mm, respectively; matrix size, 192 × 82; slice thickness, 4 mm; acquisition time, 2 minutes 47 seconds and 2 minutes 31 seconds, respectively; and 5 readout segments for rs-EPI). Apparent diffusion coefficient (ADC) maps were calculated automatically using MRI software from DWI; and (3) pre- and postcontrast, volumetric interpolated breath-hold examination sequences with a TR/TE of 4.4/1.7, flip angle of 10°, slice thickness of 1.2-mm and acquisition time of 1 minute. The images were obtained before and at 10, 70, 130, 190, 250, and 310 seconds after an injection of contrast agent gadolinium-DTPA (Gd-DTPA, 0.1 mmol/kg Gadovist; Bayer Schering Parma, Berlin, Germany). Imaging performed with a 1.5T MRI system (Signa; GE Medical Systems, Milwaukee, USA) was conducted using the following sequences: (1) axial, fat-suppressed, fast spin-echo T2-weighted imaging (TR/TE = 4,000/85, flip angle of 90°, 30 slices, FOV of 240 mm, matrix of 256 × 224, NEX of 2, 3-mm slice thickness with 0.1-mm slice gap and acquisition time of 2 minutes 56 seconds); (2) axial DWI with ss-EPI (b = 0 and 1,000 s/mm^2, TR/TE = 6,000/75, FOV of 360 mm, matrix of 128 × 128, 2 NEX, 4-mm slice thickness with 1-mm slice gap, and acquisition time of 1 minute 30 seconds); and (3) pre- and postcontrast, axial spin-echo T1-weighted imaging (TR/TE = 6.2/3.1, flip angle of 10°, 2.6 mm section thickness, FOV of 300 mm, matrix of 256 × 192, and acquisition time of 1 minute 31 seconds) obtained before and 91, 192, 273, 364, and 455 seconds after the rapid bolus injection of Gd-DTPA.

The images were retrospectively reviewed by two experienced breast radiologists and a consensus was agreed concerning the following parameters: (1) long and short axis length; (2) short diameter/long diameter (S/L) ratio; (3) presence of fatty hilum; (4) multiplicity; (5) intercostal space location; and (6) signal intensity on diffusion weighted image and ADC map. For measurement of LN size both sagittal and axial images were evaluated and the largest and the smallest lengths were measured using the magnified images on dedicated software (Aquarius iNtuition; TeraRecon Inc., Foster City, USA).

Statistical analysis

Differences in age, tumor size, short axis length of IMLN, long axis length of IMLN, and S/L ratio were tested using the independent-sample t-test. Differences in distant metastasis, fatty hilum, intercostal space, and signal intensity in DWI and ADC maps were tested using the Mann-Whitney U test (if the number in a cell was ≤ 5). Differences in axillary metastasis, LN multiplicity, and tumor location were tested using Pearson

http://dx.doi.org/10.4048/jbc.2016.19.2.191

chi-square test.

A parametric estimate of the area under the receiver operating characteristic (ROC) curve was used to compare the diagnostic ability of variables to differentiate benign and malignant lymph nodes. The optimal cutoff value was determined according to the Youden index (J), and the sensitivity, specificity, positive predictive value (PPV), and negative predictive value (NPV) were calculated. All statistical analyses were performed using the statistical software package SPSS version 19.0 (IBM Corp., Armonk, USA). A p-value <0.05 was considered statistically significant.

RESULTS

Patient characteristics

Patient characteristics are summarized in Table 1. Of all the parameters measured, only axillary LN metastasis was significantly different between benign and malignant internal mammary lymph node groups ($p<0.05$). Positive axillary lymph nodal involvement of the malignant and benign groups was 85.0% and 52.6%, respectively. The other characteristics were not significantly different between the two groups (Table 1).

Positive distant metastasis such as liver, bone, lung, brain, contralateral IMLN and contralateral axillary LN of the malignant and benign groups was 32.5% and 26.3%, respectively.

In PET/CT, the mean maximum standardized uptake value of metastatic IMLNs was 4.78 ± 3.32. No FDG uptake was observed in the benign IMLNs.

MRI findings

The relevant measurable characteristics obtained from the MRI findings are summarized in Table 2.

Of the parameters measured, short and long axis length, absent fatty hilum and restricted diffusion ($p<0.001$ for each), and S/L ratio ($p=0.041$) were all significantly different between the two groups. In the malignant IMLN group, the mean short axis length of enlarged nodes was 8.2 ± 2.9 mm and the mean long axis length was 14.5 ± 4.8 mm; the S/L ratio was 0.59 ± 0.17. Most cases lost fatty hilum (95.0%), and showed restricted diffusion (85.0%) (Figure 1, 2). In the benign IMLN group, the mean short axis length was 3.6 ± 1.3 mm and the mean long axis length was 8.1 ± 2.4 mm; the S/L ratio was 0.45 ± 0.10. All cases preserved fatty hilum (100.0%) and most did not show restricted diffusion (68.5%) (Figure 3, 4). In both groups, the majority showed single node involvement (65.0% and 68.4% for malignant and benign groups, respectively) located at the second intercostal space (42.5% and 84.2%, respectively).

Based on the ROC curves (Figure 5), short axis length was the most discriminative variable for predicting a metastatic node (AUC, 0.951). A short axis length of 4mm was determined as the threshold at which the Youden index reached its

Table 1. Patient characteristics

Characteristic	Benign IMLN (n=19) No. (%)	Malignant IMLN (n=40) No. (%)	p-value
Age (yr)*	48.7 ± 10.4	50.5 ± 10.7	0.547
Tumor size (mm)*	37.2 ± 33.4	40.6 ± 28.7	0.689
Tumor location			0.977
Lateral	11 (57.9)	23 (57.5)	
Medial	8 (42.1)	17 (42.5)	
Axillary LN metastasis			0.008
Negative	9 (47.4)	6 (15.0)	
Positive	10 (52.6)	34 (85.0)	
Distant metastasis			0.633
Negative	14 (73.7)	27 (67.5)	
Positive	5 (26.3)	13 (32.5)	

IMLN = internal mammary lymph node; LN = lymph node.
*Mean ± SD.

Table 2. Magnetic resonance imaging findings of internal mammary lymph nodes

Variable	Benign (n=19) No. (%)	Malignant (n=40) No. (%)	p-value
Short axis length (mm)*	3.6 ± 1.3	8.2 ± 2.9	0.000
Long axis length (mm)*	8.1 ± 2.4	14.5 ± 4.8	0.000
S/L ratio*	0.45 ± 0.10	0.59 ± 0.17	0.041
Fatty hilum			0.000
Absence	0	38 (95.0)	
Presence	19 (100.0)	2 (5.0)	
Multiplicity			0.795
Single	13 (68.4)	26 (65.0)	
Multiplicity	6 (31.6)	14 (35.0)	
Intercostal space			0.907
1st	1 (5.3)	10 (25.0)	
2nd	16 (84.2)	17 (42.5)	
3rd	1 (5.3)	12 (30.0)	
4th	1 (5.3)	1 (2.5)	
DWI signal intensity			0.000
Hyperintense	8 (42.1)	35 (87.5)	
Isointense	7 (36.8)	4 (10.0)	
Hypointense	1 (5.3)	0	
Unknown†	3 (15.8)	1 (2.5)	
ADC map‡			0.000
Decreased	3 (15.8)	34 (85.0)	
Isointense	12 (63.2)	4 (10.0)	
Increased	1 (5.3)	0	
Unknown†	3 (15.8)	2 (5.0)	

S/L ratio = short axis length/long axis length ratio; DWI = diffusion weighted imaging; ADC = apparent diffusion coefficient.
*Mean ± SD; †Signal intensity on DWI and ADC map could not be evaluated due to poor image quality; ‡Signal intensity on ADC map in comparison with DWI.

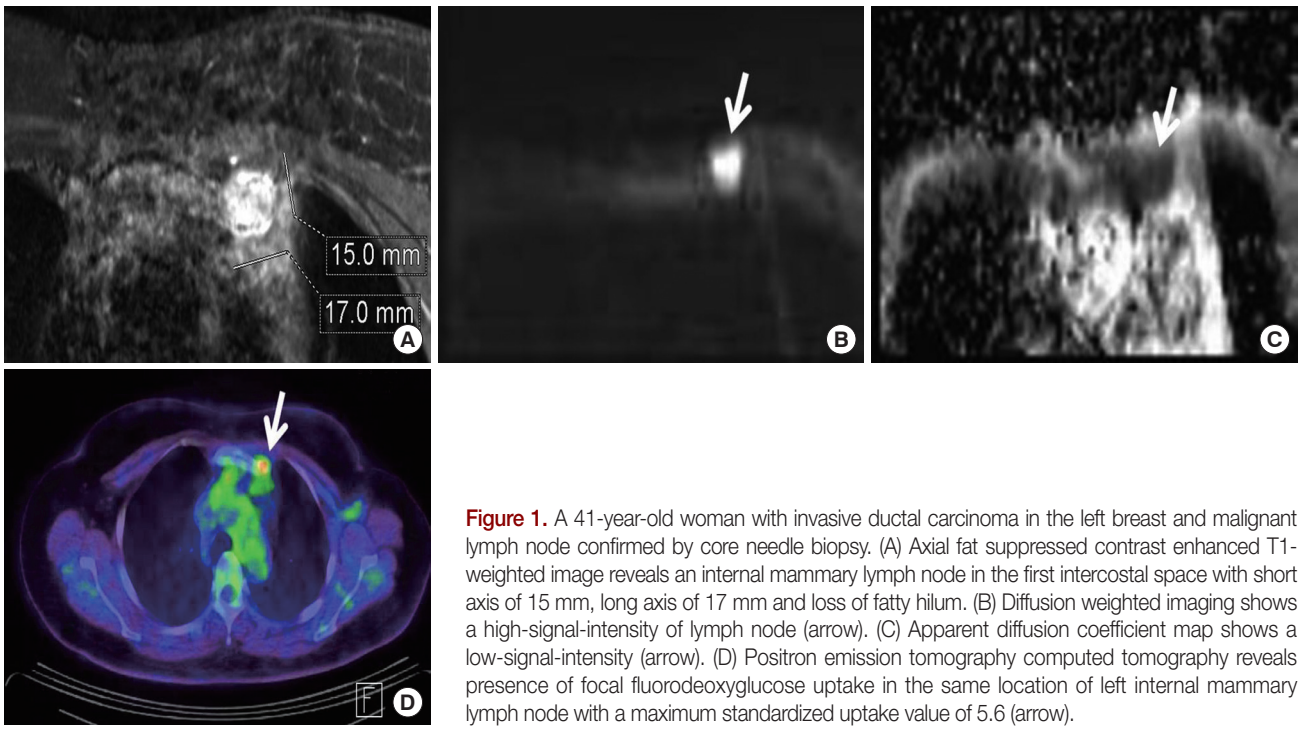

Figure 1. A 41-year-old woman with invasive ductal carcinoma in the left breast and malignant lymph node confirmed by core needle biopsy. (A) Axial fat suppressed contrast enhanced T1-weighted image reveals an internal mammary lymph node in the first intercostal space with short axis of 15 mm, long axis of 17 mm and loss of fatty hilum. (B) Diffusion weighted imaging shows a high-signal-intensity of lymph node (arrow). (C) Apparent diffusion coefficient map shows a low-signal-intensity (arrow). (D) Positron emission tomography computed tomography reveals presence of focal fluorodeoxyglucose uptake in the same location of left internal mammary lymph node with a maximum standardized uptake value of 5.6 (arrow).

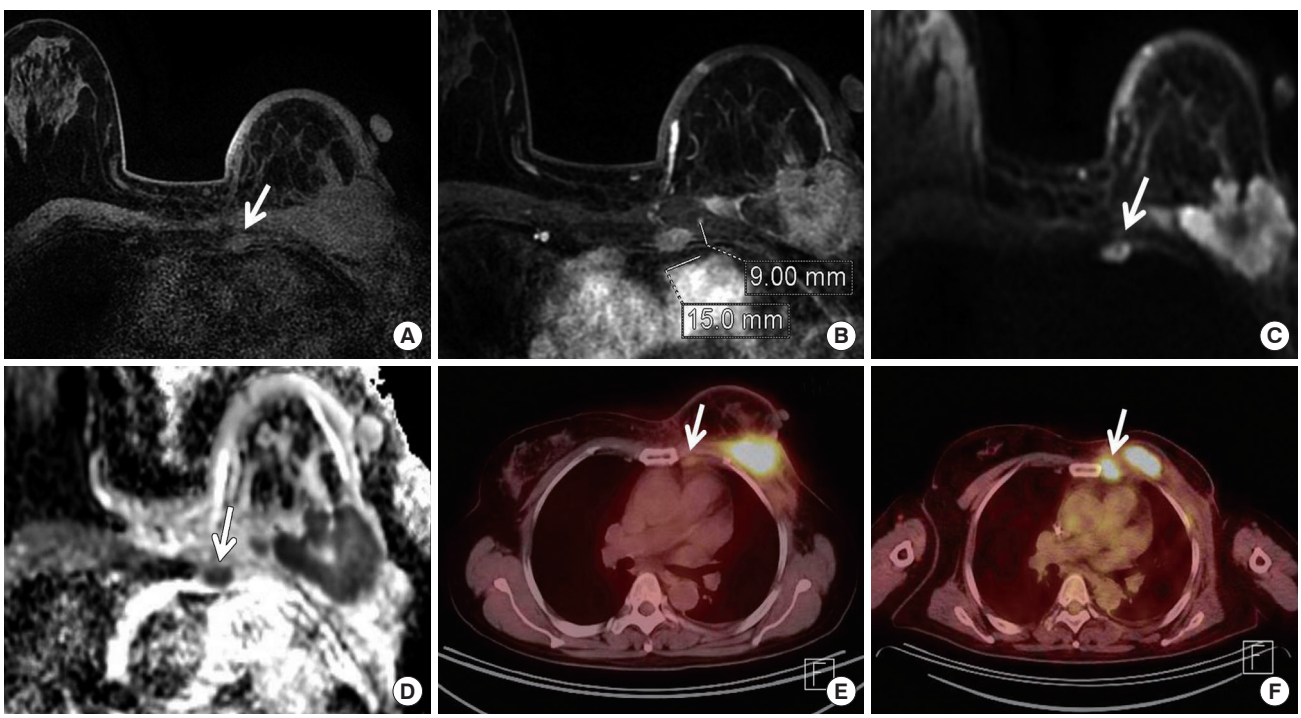

Figure 2. A 48-year-old woman with invasive ductal carcinoma in the left breast and malignant lymph node classified due to increased fluorodeoxyglucose (FDG) uptake on positron emission tomography computed tomography (PET/CT). (A) Axial fat suppressed T1-weighted image reveals an internal mammary lymph node (arrow) in the third intercostal space with loss of fatty hilum. (B) Axial fat suppressed contrast enhanced T1-weighted image, the size of lymph node is short axis of 9 mm and long axis of 15 mm. (C) Diffusion weighted imaging shows a high-signal-intensity of lymph node (arrow). (D) Apparent diffusion coefficient map shows a low-signal-intensity (arrow). (E) Initial PET/CT reveals presence of focal FDG uptake in the same location of left internal mammary lymph node with a maximum standardized uptake value of 1.5 (arrow). (F) Four months later, there is a marked increased FDG uptake from 1.5 to 7.8 (arrow).

http://dx.doi.org/10.4048/jbc.2016.19.2.191

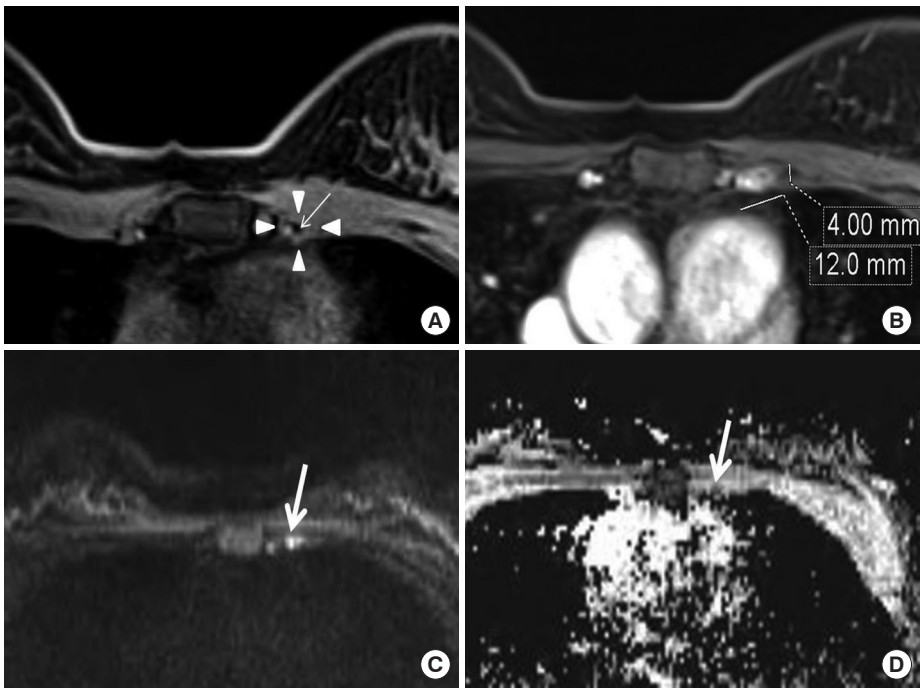

Figure 3. A 41-year-old woman with invasive ductal carcinoma in the left breast and benign lymph node confirmed by fine-needle aspiration and biopsy. (A) Axial fat suppressed T1-weighted image reveals an internal mammary lymph node (arrowheads) in the second intercostal space with preserved fatty hilum showing low-signal-intensity (arrow). (B) On axial fat suppressed contrast enhanced T1-weighted image, the size of lymph node is 4 mm (short axis) and 12 mm (long axis). (C) Diffusion weighted imaging shows a high-signal-intensity of lymph node (arrow). (D) Apparent diffusion coefficient map shows a iso-signal-intensity (arrow).

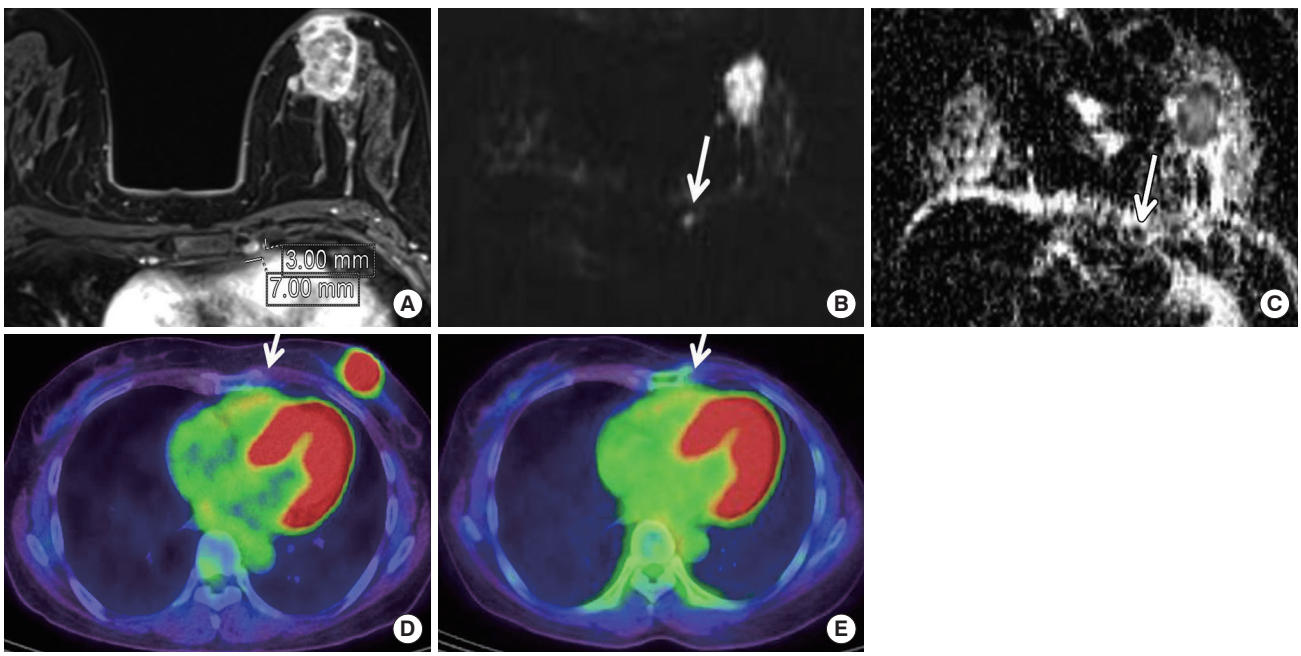

Figure 4. A 53-year-old woman with invasive ductal carcinoma in the left breast and benign lymph node (LN) classified due to no fluorodeoxyglucose (FDG) uptake on positron emission tomography computed tomography (PET/CT). (A) Axial fat suppressed contrast enhanced T1-weighted image reveals an internal mammary LN in the second intercostal space with short axis of 3 mm, long axis of 7 mm and preserved fatty hilum. (B) Diffusion weighted imaging shows a high-signal-intensity of LN (arrow). (C) Apparent diffusion coefficient map shows a low-signal-intensity (arrow). Initial (D) and after 1 year and 1 month (E) PET/CT reveals absence of focal FDG uptake in the same location of left internal mammary LN (arrow).

Table 3. Diagnostic performance of continuous magnetic resonance imaging parameters of internal mammary lymph nodes

Variable	AUC	95% CI	*p*-value*	Threshold	Youden index	Se (%)	Sp (%)	PPV (%)	NPV (%)
Short axis length (mm)	0.951	0.861–0.990	<0.001	>4	0.7671	92.5	84.2	92.5	84.2
Long axis length (mm)	0.906	0.801–0.966	<0.001	>10	0.6447	75.0	89.5	93.7	63.0
S/L ratio	0.756	0.627–0.858	<0.001	>0.5	0.5171	67.5	84.2	90.0	55.2

AUC = area under the receiver operating characteristics (ROC) curve; CI = confidence interval; Se = sensitivity; Sp = specificity; PPV = positive predictive value; NPV = negative predictive value; S/L ratio = short axis length/long axis length ratio.
*ROC curve analysis for variables to differentiate benign and malignant lymph nodes.

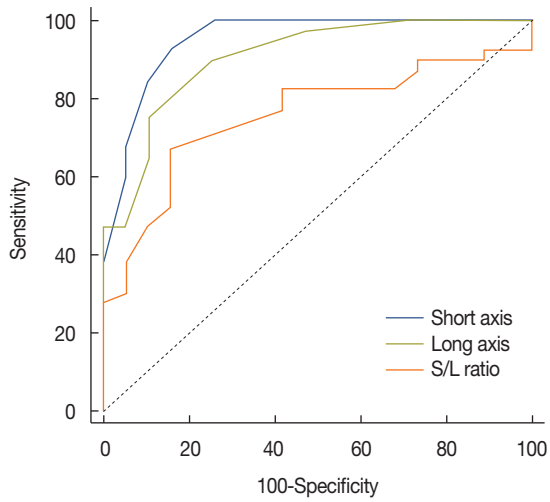

Figure 5. Receiver operating characteristic curves for the individual evaluated magnetic resonance imaging parameters of the internal mammary lymph node. The area under the receiver operating characteristics curve of short axis length, long axis length and short axis length/long axis length (S/L) ratio were 0.951, 0.906, and 0.756, respectively.

peak. At the determined threshold, the sensitivity, specificity, PPV, and NPV were 92.5%, 84.2%, 92.5%, and 84.2%, respectively. The AUC of long axis length and S/L ratio were 0.906 and 0.756, respectively. The thresholds for each parameter and the sensitivity, specificity, PPV, and NPV at the adopted thresholds are summarized in Table 3.

DISCUSSION

Our study evaluated the ability of MRI features to discriminate between malignant and benign IMLNs in breast cancer patients. Short axis length, long axis length, S/L ratio, absent fatty hilum, and restricted diffusion were discriminative variables for predicting metastatic nodes. Among these, short axis length was the most discriminative variable. The optimal threshold to predict metastasis was 4 mm for short axis length and 10 mm for long axis length, respectively. Kim et al. [11] reported optimal thresholds for short and long axis lengths of axillary LN as 9.3 mm and 11.3 mm, respectively. In the present study, the short axis length was considerably shorter than that of axillary LN and the long axis length was slightly shorter than that of axillary LN. In recent studies of normal internal mammary lymph nodes incidentally detected on breast MRI, the average long axis diameter was 4.5 mm (range, 2–9 mm) [12] or 4 mm (range, 3–10 mm) [13].

Mean S/L ratio was higher in malignant nodes (0.59 ± 0.17) than benign nodes (0.45 ± 0.10), and the optimal threshold was 0.5. This finding suggests that benign nodes tend to be more lentiform in shape and malignant nodes tend to be more round. Other studies of axillary LNs have reported a significant difference in the short axis–long axis ratio [14,15]. He et al. [14] reported that the S/L axis ratio of axillary malignant and benign nodes was, respectively, 0.71 ± 0.12 versus 0.55 ± 0.16 (p < 0.001) and the optimal threshold was 0.62.

Fatty hilum was absent in the majority of malignant nodes (95.0%), while all benign nodes (100.0%) preserved fatty hilum (p < 0.001). Loss of fatty hilum also varied significantly in other studies of axillary LNs [11,15-17].

Diffusion restriction was observed in the majority of malignant nodes (85.0%) and only 15.8% of benign nodes (p < 0.001). These results are similar to those of prior studies of axillary LNs [11,14,18-20] .

Previous studies have demonstrated that PET/CT is superior to conventional diagnostic techniques for detection of internal mammary LN metastases [21,22]. An et al. [7] reported that PET/CT-positive internal mammary LNs were defined as those with an uptake greater than the adjacent background activity of the pectoralis muscle or the intercostal space along the lateral sternal border. In their study, there were statistically significant differences in maximum standardized uptake values from PET/CT between the metastatic and benign IMLN groups (p = 0.002), the mean maximum standardized uptake value of metastatic and benign IMLNs being 3.53 ± 1.79 and 1.06 ± 1.09, respectively. Seo et al. [10] reported that most metastatic LNs (83.0%) present with a higher intensity of FDG uptake than the mediastinal blood pool, with a maximum standardized uptake of 3.5 ± 4.3. In our study, the mean maximum standardized uptake value of metastatic IMLNs

http://dx.doi.org/10.4048/jbc.2016.19.2.191

was 4.78 ± 3.32.

For patient characteristics, axillary LN metastasis was significantly different between the two groups ($p < 0.05$). Previous studies report that positivity of axillary nodes is the strongest predictive factor for IMLN involvement [23,24]. Tumors with a medial location and larger size are associated with a higher rate of internal mammary LN metastases [25-28]. However, contrary to previous results, medial tumor location and tumor size were not predictive for internal mammary LN metastases in our present analysis. Coombs et al. [29] reported age under 35 years as a risk factor for IMLN involvement. Hence, it is important to note that the patients in our malignant group were older than those in our benign group.

There are some limitations to the present study. First, it was a retrospective study with a small case number. Second, IMLN malignancy was mostly defined by increased maximum standardized uptake value and not by pathology. Third, lymph nodes with a long axis length of less than 5 mm were not included.

In conclusion, MRI parameters including short axis length, long axis length, S/L ratio, absent fatty hilum, and restricted diffusion can be used to differentiate malignant and benign IMLN in breast cancer patients. Among these parameters, short axis length was the most discriminative variable for predicting metastatic nodes.

CONFLICT OF INTEREST

The authors declare that they have no competing interests.

REFERENCES

1. Li Z, Gu X, Tong J, Liu B, Sun L, Gao X, et al. A meta-analysis of internal mammary lymph node metastasis in breast cancer patients. Onkologie 2013;36:747-52.
2. Cody HS 3rd. Clinical significance and management of extra-axillary sentinel lymph nodes: worthwhile or irrelevant? Surg Oncol Clin N Am 2010;19:507-17.
3. Veronesi U, Marubini E, Mariani L, Valagussa P, Zucali R. The dissection of internal mammary nodes does not improve the survival of breast cancer patients: 30-year results of a randomised trial. Eur J Cancer 1999;35:1320-5.
4. Cranenbroek S, van der Sangen MJ, Kuijt GP, Voogd AC. Diagnosis, treatment and prognosis of internal mammary lymph node recurrence in breast cancer patients. Breast Cancer Res Treat 2005;89:271-5.
5. Maalej M, Gargouri W, Kochbati L, Nasr C, Frikha H, Hentati D, et al. Internal mammary lymph node invasion in breast cancer: myth or reality? Tunis Med 2009;87:319-22.
6. Noguchi M. Internal mammary sentinel node biopsy for breast cancer: is it practicable and relevant? (Review). Oncol Rep 2002;9:461-8.
7. An YY, Kim SH, Kang BJ, Lee AW. Comparisons of positron emission tomography/computed tomography and ultrasound imaging for detection of internal mammary lymph node metastases in patients with breast cancer and pathologic correlation by ultrasound-guided biopsy procedures. J Ultrasound Med 2015;34:1385-94.
8. Chen RC, Lin NU, Golshan M, Harris JR, Bellon JR. Internal mammary nodes in breast cancer: diagnosis and implications for patient management: a systematic review. J Clin Oncol 2008;26:4981-9.
9. Kinoshita T, Odagiri K, Andoh K, Doiuchi T, Sugimura K, Shiotani S, et al. Evaluation of small internal mammary lymph node metastases in breast cancer by MRI. Radiat Med 1999;17:189-93.
10. Seo MJ, Lee JJ, Kim HO, Chae SY, Park SH, Ryu JS, et al. Detection of internal mammary lymph node metastasis with (18)F-fluorodeoxyglucose positron emission tomography/computed tomography in patients with stage III breast cancer. Eur J Nucl Med Mol Imaging 2014;41:438-45.
11. Kim EJ, Kim SH, Kang BJ, Choi BG, Song BJ, Choi JJ. Diagnostic value of breast MRI for predicting metastatic axillary lymph nodes in breast cancer patients: diffusion-weighted MRI and conventional MRI. Magn Reson Imaging 2014;32:1230-6.
12. Mack M, Chetlen A, Liao J. Incidental internal mammary lymph nodes visualized on screening breast MRI. AJR Am J Roentgenol 2015;205:209-14.
13. Ray KM, Munir R, Wisner DJ, Azziz A, Holland BC, Kornak J, et al. Internal mammary lymph nodes as incidental findings at screening breast MRI. Clin Imaging 2015;39:791-3.
14. He N, Xie C, Wei W, Pan C, Wang W, Lv N, et al. A new, preoperative, MRI-based scoring system for diagnosing malignant axillary lymph nodes in women evaluated for breast cancer. Eur J Radiol 2012;81:2602-12.
15. Yoshimura G, Sakurai T, Oura S, Suzuma T, Tamaki T, Umemura T, et al. Evaluation of axillary lymph node status in breast cancer with MRI. Breast Cancer 1999;6:249-58.
16. Luciani A, Dao TH, Lapeyre M, Schwarzinger M, Debaecque C, Lantieri L, et al. Simultaneous bilateral breast and high-resolution axillary MRI of patients with breast cancer: preliminary results. AJR Am J Roentgenol 2004;182:1059-67.
17. Mortellaro VE, Marshall J, Singer L, Hochwald SN, Chang M, Copeland EM, et al. Magnetic resonance imaging for axillary staging in patients with breast cancer. J Magn Reson Imaging 2009;30:309-12.
18. Fornasa F, Nesoti MV, Bovo C, Bonavina MG. Diffusion-weighted magnetic resonance imaging in the characterization of axillary lymph nodes in patients with breast cancer. J Magn Reson Imaging 2012;36:858-64.
19. Junping W, Tongguo S, Yunting Z, Chunshui Y, Renju B. Discrimination of axillary metastatic from nonmetastatic lymph nodes with PROPELLER diffusion-weighted MR imaging in a metastatic breast cancer model and its correlation with cellularity. J Magn Reson Imaging 2012;36:624-31.
20. Wang J, Liao Q, Zhang Y, Yu C, Bai R, Sun H. Differential diagnosis of axillary inflammatory and metastatic lymph nodes in rabbit models by using diffusion-weighted imaging: compared with conventional magnetic resonance imaging. Korean J Radiol 2012;13:458-66.
21. Eubank WB, Mankoff DA, Takasugi J, Vesselle H, Eary JF, Shanley TJ, et al. 18Fluorodeoxyglucose positron emission tomography to detect mediastinal or internal mammary metastases in breast cancer. J Clin Oncol

2001;19:3516-23.
22. Segaert I, Mottaghy F, Ceyssens S, De Wever W, Stroobants S, Van Ongeval C, et al. Additional value of PET-CT in staging of clinical stage IIB and III breast cancer. Breast J 2010;16:617-24.
23. Hindié E, Groheux D, Hennequin C, Zanotti-Fregonara P, Vercellino L, Berenger N, et al. Lymphoscintigraphy can select breast cancer patients for internal mammary chain radiotherapy. Int J Radiat Oncol Biol Phys 2012;83:1081-8.
24. van der Ent FW, Kengen RA, van der Pol HA, Povel JA, Stroeken HJ, Hoofwijk AG. Halsted revisited: internal mammary sentinel lymph node biopsy in breast cancer. Ann Surg 2001;234:79-84.
25. Donegan WL. The influence of untreated internal mammary metastases upon the course of mammary cancer. Cancer 1977;39:533-8.
26. Huang O, Wang L, Shen K, Lin H, Hu Z, Liu G, et al. Breast cancer subpopulation with high risk of internal mammary lymph nodes metastasis: analysis of 2,269 Chinese breast cancer patients treated with extended radical mastectomy. Breast Cancer Res Treat 2008;107:379-87.
27. Lacour J, Bucalossi P, Cacers E, Jacobelli G, Koszarowski T, Le M, et al. Radical mastectomy versus radical mastectomy plus internal mammary dissection: five-year results of an international cooperative study. Cancer 1976;37:206-14.
28. Livingston SF, Arlen M. The extended extrapleural radical mastectomy: its role in the treatment of carcinoma of the breast. Ann Surg 1974;179:260-5.
29. Coombs NJ, Boyages J, French JR, Ung OA. Internal mammary sentinel nodes: ignore, irradiate or operate? Eur J Cancer 2009;45:789-94.

http://dx.doi.org/10.4048/jbc.2016.19.2.191